Interlayer interactions and the dependence of biaxiality of the chiral smectic-C^* phase on electric field in the helical unwinding process

Jang-Kun Song,[1] J. K. Vij,[1,*] and Ichiro Kobayashi[2]
[1]*Department of Electronic and Electrical Engineering, Trinity College, University of Dublin, Dublin 2, Ireland*
[2]*Nissan Chemical Industries, Ltd., 722-1, Tsuboi-Cho, Funabashi-shi, Chiba 274-8507, Japan*
(Received 22 August 2006; revised manuscript received 17 January 2007; published 22 May 2007)

We investigate the unwinding process of pure and racemized mixtures of (1-methylheptyloxycarbonyl) phenyl-4′-carboctyloxy-biphenyl-4-carboxylate (MHPOOCBC) in homeotropic cells by studying (i) the optical texture under crossed polarizers and (ii) the tilted conoscopy as a function of the electric field for different temperatures. The tilted conoscopy yields biaxiality and the tilt angle for values of the latter up to 45°. We find that the unwinding process depends on the optical purity of the sample and the temperature. A cell with pure MHPOOCBC surprisingly exhibits a large positive biaxiality in the initial stages of the unwinding process. The magnitude of the positive biaxiality decreases with a decrease in the enantiomeric excess (EE) of the compound and eventually it becomes negative for a material having a low EE value. The negative biaxiality observed in a mixture with a low EE value is normal and can be explained by a double sine-Gordon equation proposed by Meyer. Microscopic observations show that the special unwinding behavior (positive biaxiality) is related to the helical fractures, that is, to the existence of discretely coiled helical structures. We show that these helical fractures arise from the existence of a narrow energy well in the synclinic position. This implies that the elastic constant near the synclinic position is significantly larger than in other positions. By adopting a semiempirical equation for the interlayer interactions which replaces the conventional equation, we successfully simulate the various unwinding behaviors. We reasonably conclude that the special interlayer interaction is due to the steric interactions between the two adjacent surfaces formed by somewhat tilted terminal parts of the molecules.

DOI: 10.1103/PhysRevE.75.051705 PACS number(s): 61.30.Gd, 42.70.Df, 77.84.Nh

I. INTRODUCTION

Smectic liquid crystals are composed of smectic layers forming two-dimensional liquids, where the long molecular axes are highly ordered and tilted with respect to the layer normal in tilted smectic phases. The core parts of the molecules are located in the centers of layers and the terminal parts are located near the surfaces, and these are in contact with the terminal parts of the molecules in an adjacent layer. The **c** directors of the two neighboring layers, which are the projections of the directors onto the layer, could be parallel in ferroelectric liquid crystals (FLC), antiparallel in antiferroelectric liquid crystallic phase (AFLC), or highly twisted (smectic-$C^*\alpha$ and other subphases) [1]. The various interlayer interactions, including steric, dipole-dipole, flexoelectric, and elastic, may cause the generation of various phases in smectic liquid crystals [1,2]. Until now, many studies of the tilted smectic phases have been carried out to determine, theoretically or experimentally, how the interlayer interactions contribute to the formation of various phases at different temperatures [3,4]. In this paper, we have focused on the field-induced unwinding process [5–14] in the chiral smectic-C phase (SmC^*), because, during the unwinding process, some in-layer directors in the adjacent layers may experience a change from synclinic back to synclinic through an anticlinic order with the adjacent layer, that is, from $\Delta\phi=0$ to $\Delta\phi=2\pi$. By observing the unwinding process, we may be able to understand the interlayer interactions.

A conoscopic experiment can give information about the averaged refractive index ellipsoid of the cell [11], which is related to the molecular distribution in the cell, and so it has been used to determine the phases and the molecular distribution [11,12]. Suwa *et al.* [13,14] used conoscopy to investigate the unwinding process in MHPOBC and a short-pitch chiral smectic mixture, and they found two different types of unwinding behavior, having negative and positive biaxiality during the intermediate unwinding process. They suggested that the high positive biaxiality is quite an unexpected result and can be attained under a special distribution of the directors, a set of discrete **c** directors. However, they could not explain successfully the mechanism by which such special distributions are obtained. We used a conoscopic method with tilted cells [7,8], which gives an improved observable range of biaxiality and of the tilt angle compared to the conventional conoscopic method reported so far in the literature. We found various unwinding behaviors in (1-methylheptyloxycarbonyl)phenyl-4′-carboctyloxy-biphenyl-4-carboxylate (MHPOOCBC) and its racemized mixtures, depending on the racemization ratio and the temperature. Pure MHPOOCBC and mixtures with large enantiomeric excess (EE) show large positive biaxiality during the intermediate unwinding process, whereas the mixtures with low EE show negative biaxiality during the early stages of the unwinding process. Microscopic observations showed that the various behaviors are due to discontinuous **c** directors, which may be similar to the discrete structure suggested by Suwa *et al.* [14]. The aim of this paper is to explain the emergence of the various unwinding behaviors by a

*Email address: jvij@tcd.ie

 ©2007 The American Physical Society

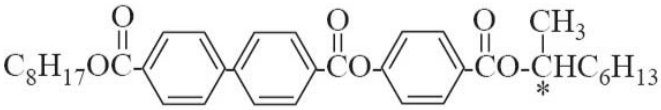

FIG. 1. Chemical structure of (1-methylheptyloxycarbonyl) phenyl-4′-carboctyloxy-biphenyl-4-carboxylate (MHPOOCBC) ($\mathrm{Sm}C^*_\gamma \overset{42\,^\circ\mathrm{C}}{\rightleftharpoons} \mathrm{Sm}C^* \overset{87\,^\circ\mathrm{C}}{\rightleftharpoons} \mathrm{Sm}A$ [1]). Pure MHPOOCBC and its racemic mixtures (EE=0.3,0.7) were used for experiments.

new model and to estimate the azimuthal-angle-dependent interlayer interaction energy in the ferroelectric phase.

II. CONOSCOPIC AND MICROSCOPIC EXPERIMENTS

The liquid crystal (LC) samples used are MHPOOCBC, whose structure is shown in Fig. 1, and its racemic mixtures, whose racemization ratios or enantiomeric excess ratios defined as $(R-S)/(R+S)$, are 0.3 and 0.7. Pure MHPOOCBC has a wide temperature range of the SmC^* and SmC^*_γ phases at low temperatures [1].

Homeotropically aligned cells having 100–150 μm thicknesses were prepared by using two indium tin oxide–glass plates coated with a silane coupling agent [Dow-Corning silane, 72% 3-(trimethoxysilyl)propyldimethyloctadecyl ammonium chloride and 28% MeOH]. Biaxiality was studied by conoscopy with a tilted cell [7,8], which allowed us to measure LC materials having large tilt angles and large biaxiality. All conoscopic observations were made using an optical polarizing microscope (Olympus BX-52) having large numerical aperture (NA) lenses for both the objective (Olympus, LM PlanFI, 50X/0.5NA) and the condenser. A NA of 0.5 corresponds to an angular field extending from −30° to 30° in air, and extending from −19.5° to 19.5° in a liquid crystal cell with $n_{\mathrm{LC}}=1.5$ placed horizontally. Consequently, the melatopes of MHPOOCBC having tilt angles of ~25° are out of the field of view, so that we could not determine the biaxiality.

By sandwiching the cell between a pair of prisms (Fig. 2) made of heavy optical glass SF11 (index of refraction of 1.82) and having an apex angle of 30°, we attained an angular field that extends from 17° to 60.6°, so that a large tilt angle and large biaxiality could be measured. Index-of-refraction matching oil was used to reduce the reflection arising from the air gaps between the glass plates and the prisms. Sometimes the prism was replaced with a conventional cell and its metal attachments slanted by 30° with respect to the microscope stage so that the angular field in the liquid crystalline sample extends from 0° to 35.3°. By combining the two methods, we can use conoscopy for measuring the biaxiality when the tilt angle is as large as 45°. The sample was heated in an oven.

Snell's law assures that a ray traveling in air at an angle of θ_{air} with respect to the microscope optical axis makes an angle θ_{LC} with the smectic layer normal given by

$$\theta_{\mathrm{LC}} = \sin^{-1}\left\{\sin\left[\sin^{-1}\left(\frac{\sin\theta_{\mathrm{air}}}{n_{\mathrm{pr}}}\right)+\alpha\right]\frac{n_{\mathrm{pr}}}{n_{\mathrm{LC}}}\right\}. \quad (1)$$

Here n_{pr} and α are the index of refraction of the prism and its apex angle, and n_{LC} is the index of refraction of the liquid crystalline sample. This equation obtained for the prism-sandwiched cell is also applicable to a slanted cell and a conventional cell placed horizontally on the microscope stage, where α is 30° and zero, respectively, and $n_{\mathrm{pr}}=1$ for both cases.

We applied an electric field using polythelthylene terephthalate (PET) spacers covered with gold foil spaced 300 μm apart. A wave generator and an amplifier allowed us to apply a maximum voltage of 600 V dc or ac to the sample cell. The quality of the conoscopic image deteriorated seriously when some LC flow occurred. To minimize the flow effect, we were very careful in sample handling and utilized a 1 Hz square wave field instead of applying dc voltage.

The obtained conoscopic images were analyzed to get the biaxiality (n_Y-n_X) and the tilt angle (θ), where the Z axis is parallel to the long axis of the refractive index ellipsoid, the X and Z axes are in the tilt plane, and the Y axis is perpendicular to the tilt plane. Strictly speaking, biaxiality can be obtained only in the case of a single biaxial plate such as a perfectly unwound smectic cell. In the intermediate state of unwinding in a smectic cell using long-helical-pitch materials, the molecular distribution in the cell has a very complicated semicoiled structure, and usually produces blurred conoscopic images where the optical axes are not clear. However, if the pitch is short enough, the light experiences the averaged refractive indices of the complex distribution of molecules, and conoscopy shows single-biaxial-plate-like melatopes [13,14]. Our analysis was carried out on the basis

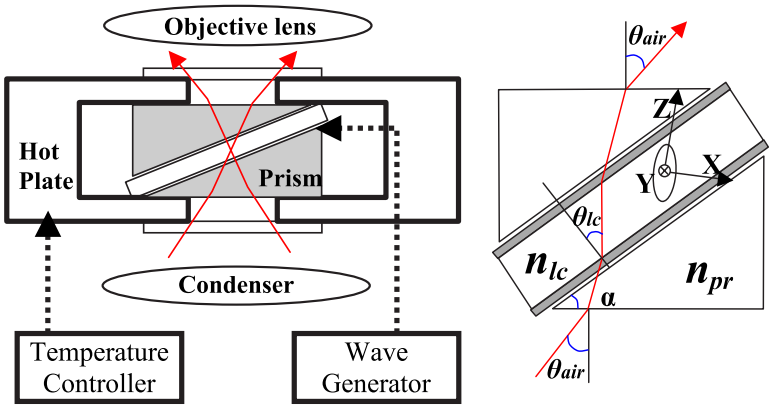

FIG. 2. (Color online) Modified conoscopic method using a tilted cell (left) and a cell sandwiched with prisms (right). X, Y, and Z axes are the eigenaxes of the refractive index ellipsoid in the cell.

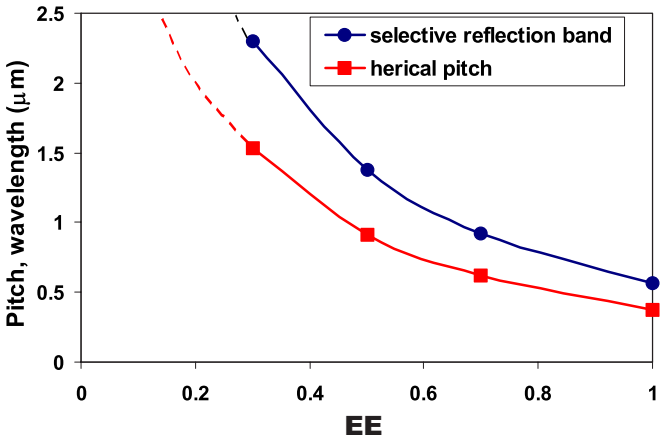

FIG. 3. (Color online) Helical pitch as a function of the EE value of the MHPOOCBC racemic mixtures (80 °C). Dashed lines show extrapolation of the experimental data.

of the approximation of the molecular distribution in the cell as that of a single biaxial plate. The racemic mixtures of MHPOOCBC having EE values of 1.0 (pure MHPOOCBC), 0.7, and 0.3 have pitch values varying from about 360 to 400 nm, 580 to 640 nm, and 1490 to 1570 nm, respectively, as seen in Fig. 3. (Here, we assumed $n_{\mathrm{LC}}=1.5$, which is needed for deducing the pitch from the selective reflection band.) Thus, the pitch of the mixture of EE 0.3 is much longer than the wavelength of light. To assure the validity of the single-plate approximation in this case, we carried out a few additional simulations, and concluded that the cell having an EE value of 0.3 also could be regarded as a single biaxial plate approximately. Details of the simulations will be shown in Sec. IV.

The method of analysis to get the biaxiality and the tilt angle on the basis of the averaged indices method is basically the same as that used by Gorecka *et al.* [11]. By assuming the minimum refractive index $n_{\mathrm{min}}=1.5$ of the system, we can obtain two other refractive indices $(n_{\mathrm{mdl}}, n_{\mathrm{max}})$ along the two eigenaxes. For this, we needed the two angles $(\theta_{o1}, \theta_{o2})$ that the two optical axes make with the layer normal, and θ_m, which is the angle that the direction of the mth dark ring from the center of the ellipsoid makes with the long axis of the refractive index ellipsoid. The mth dark point must lie in the optical plane, i.e., the plane containing the two optical axes. Usually the second dark position was selected for convenience. The angle (θ) of the long axis of the refractive index ellipsoid with the layer normal is the average of the angles that the two optical axes make with the layer normal and is written as

$$\theta = \frac{\theta_{o1} + \theta_{o2}}{2}. \tag{2}$$

The difference in the two eigen refractive indices (Δn) at any dark ring of conoscopic images can be written as

$$\Delta n = \frac{m\lambda}{l}, \tag{3}$$

where l is the length of the sample through which the light passes, and at the optical axis m becomes 0. When the optical ray lies in the plane containing the two optical axes and this makes an angle Θ with the long axis of the refractive index ellipsoid, Δn can be written as

$$\Delta n = 1 \Bigg/ \left[\left(\frac{\cos\Theta}{n_{\mathrm{max}}} \right)^2 + \left(\frac{\sin\Theta}{n_{\mathrm{min}}} \right)^2 \right]^{1/2} - n_{\mathrm{mdl}}. \tag{4}$$

By setting the two conditions (Θ=the angle that an optical axis makes with the long axis of the refractive index ellipsoid, $m=0$) and ($\Theta=\theta_m$, $m=2$ for the case of the second ring) to Eqs. (3) and (4), we can find n_{max} and n_{mdl}. If the two optical axes and the layer normal are in the same plane, that is, in the case of positive biaxiality, $n_Y=n_{\mathrm{mdl}}$ and $n_X=n_{\mathrm{min}}$, and if not, $n_Y=n_{\mathrm{min}}$ and $n_X=n_{\mathrm{mdl}}$ in the case of negative biaxiality. Gorecka *et al.* [11] used an approximated equation instead of Eq. (4).

Figure 4 shows the experimental results of conoscopy. The graphs on the left-hand side are the plots of biaxiality, and those on the right are those for the tilt angle for the optically pure MHPOOCBC and its racemized mixtures. The results are shown for EE values of 0.3, 0.7, and 1 in Figs. 4(a)–4(c), respectively. Each of these figures is split into two for the biaxiality and the tilt angle results, respectively. Each plot contains several data sets measured for different temperatures. Mixture (a) (EE=0.3) shows negative biaxiality in the intermediate state of unwinding, while the two others (EE=0.7, 1.0) show large positive biaxiality. The trend depends on the temperature as well, as seen in mixtures (b) and (c); the curve for 80 °C in (b1) shows the same trend as those in (a1). Similarly, the large positive biaxiality value decreases with temperature in (c1). The tilt angle graphs show interesting behaviors as well. The tilt angle of the mixture in (a2) increases continuously with the applied voltage, but pure MHPOOCBC (c2) has a two-step increase corresponding to the increasing and decreasing parts of the biaxiality curve. Mixture (b) shows an intermediate trend. As Suwa *et al.* [13,14] correctly pointed out, the positive biaxiality cannot be explained by the conventional model, details of which will be described in the next section. Racemization affects only the spontaneous polarization and the pitch, but not the tilt angle or the quadrupolar order parameter [8]. The spontaneous polarization plays a role in initiating the unwinding process. It may affect the critical voltage for reaching a perfectly unwound state, but should not affect the trend of biaxiality as a function of the applied voltage. The pitch also affects the critical voltage, but not the unwinding trend. It is very interesting to investigate the reasons for the differences in the unwinding process realized by varying the racemization ratio.

The discrete **c** director defects can lead to a special unwinding process. The discrete directors are accompanied by domain walls in homeotropic cells and free-standing films [15–18]. Usually, for observation of the domain walls, thin free-standing films of the SmC phase have been used, because thin films having just a few smectic layers could provide more clear observation, and a longitudinal polarization of the surface layer can be used for generating the domain walls. However, Cladis *et al.* [15] noticed that discrete **c** director defects appear in chiral SmC^* cells as well. The

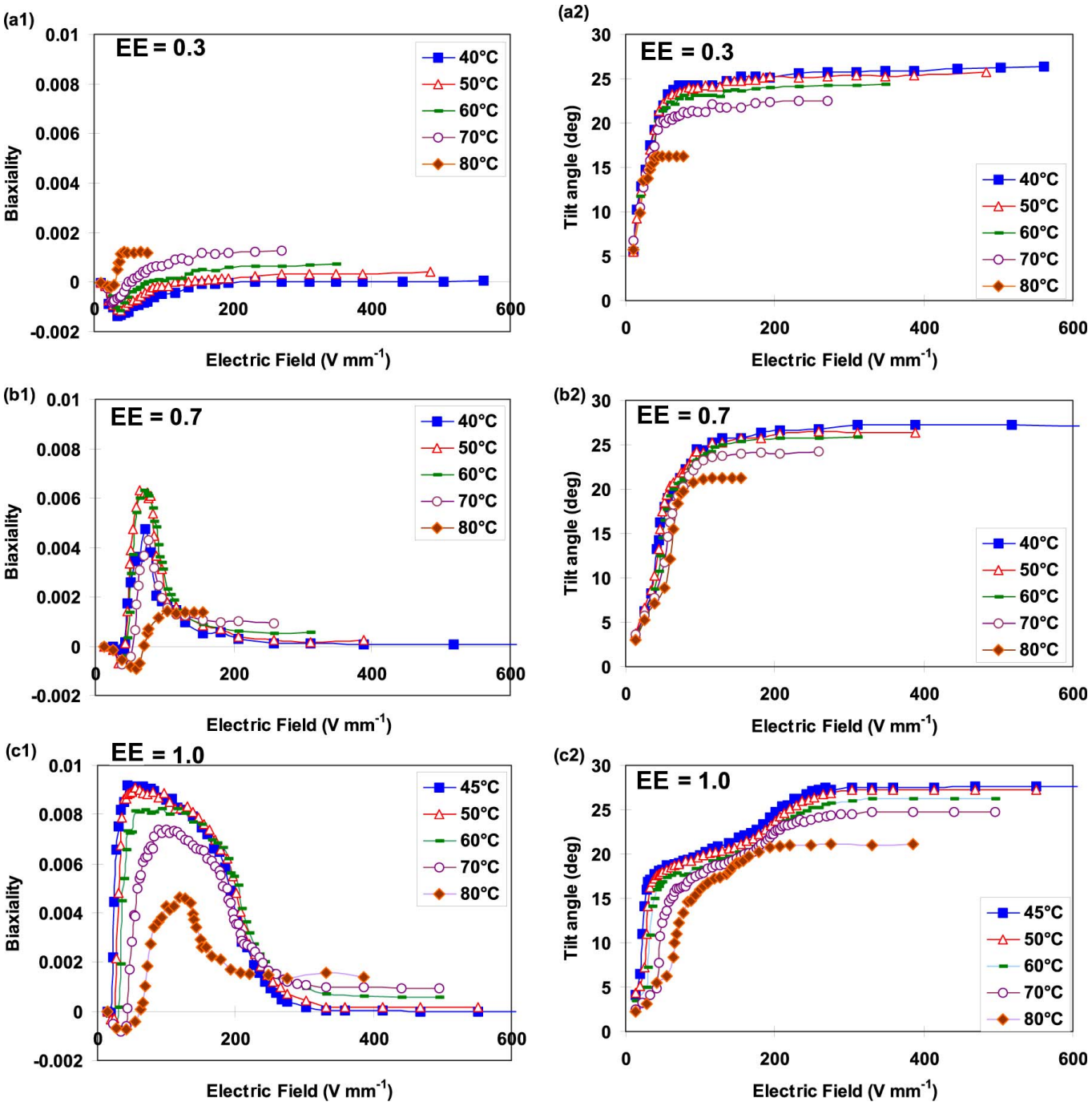

FIG. 4. (Color online) Results of the conoscopic measurements. Left: Plots of the biaxiality $(n_Y - n_X)$ vs voltage. Right: plots of the tilt angle vs voltage at various temperatures; EE=(a) 0.3, (b) 0.7, and (c) 1. Here, the enantiomeric excess (EE)$=(R-S)/(R+S)$.

domain walls they observed in the films are usually 2π or π walls, which are stabilized at the synclinic or anticlinic minimum state. 2π walls have a double dark line under cross polarizers (sometimes four dark lines) and there is no difference in the relative angles of two adjacent layers $(\Delta\phi)$ between the two domains separated by the walls, which means that 2π walls need not be accompanied by discrete **c** directors. On the other hand, lower than 2π walls, one example of which is a π wall, have a single dark line (it can rarely be a double line) and are always accompanied by discrete **c** directors, because $\Delta\phi$ of the two domains separated by the walls are different, which means at least one of the two domains has a discrete **c** director [17]. It is not easy to generate such a wall by a low field in SmC^* cells. In Eq. (6) in the next section, the elastic energy is proportional to $d\phi^2$ and so $d\phi$ should increase continuously with applied field to compensate for the ferroelectric coupling. No sudden jump in $d\phi$ occurs at a low field.

We examined micrographs to obtain a better understanding of the concept of discrete **c** directors in the SmC^* phase. Figures 5 and 6 show microscopic images of 15 μm homeotropic cells taken under crossed polarizers (the polarizer di-

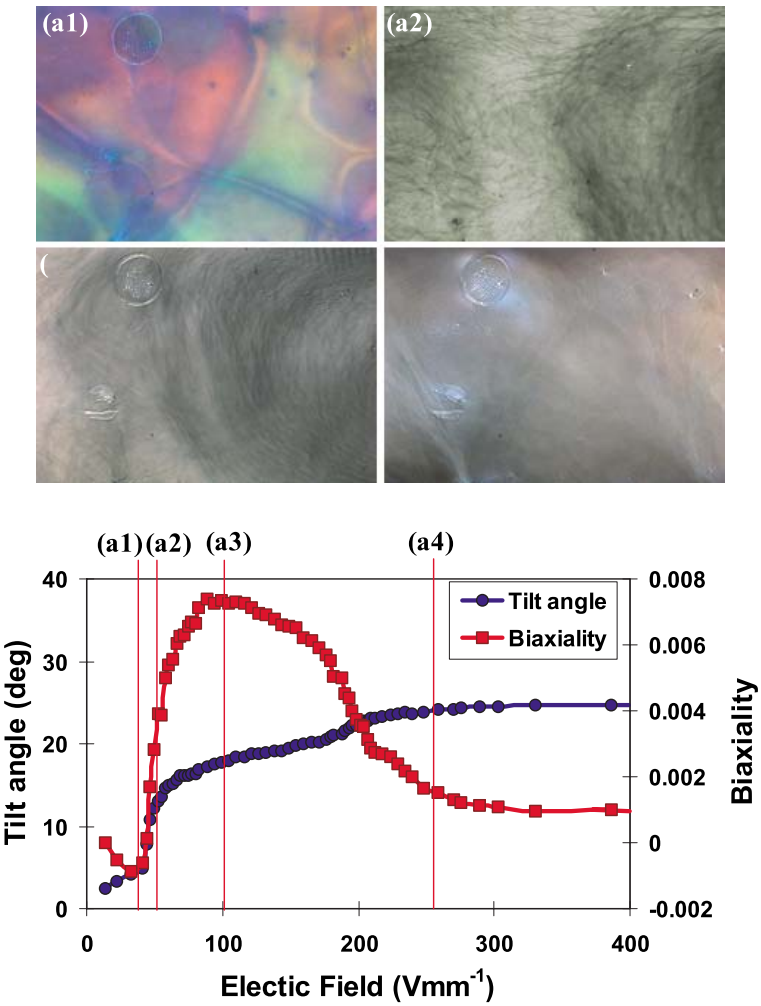

FIG. 5. (Color online) Micrographs (×200) of a homeotropic cell with pure MHPOOCBC at 70 °C in SmC^* phase: (a1) 40; (a2) 50; (a3) 100; (a4) 250 V/mm. The exposure time was adjusted to capture the best quality of the images. The biaxiality and the tilt angle graphs are from Fig. 4.

rections are parallel and perpendicular to the direction of the applied field), where the temperature was 70 °C and 1 Hz ac square voltage was applied. The images (a1)–(a4) in Fig. 5 were taken at applied fields of 40, 50, 100, and 250 V/mm, respectively, with a cell containing pure MHPOOCBC, and the images (b1)–(b4) in Fig. 6 were taken at 36, 54, 107, and 375 V/mm, respectively, in a cell with racemized MHPOOCBC (EE=0.3). The exposure time of the camera (Leica, DF480) was adjusted for each image so as to obtain pictures that can better show the domain walls. Hence the brightnesses of the images cannot be compared with each other. It may be better first to examine the cell with a racemized mixture, which is closer to a general case (Fig. 6). The homeotropic cell with such a mixture had a uniform single domain in the smectic-*A* phase (Sm*A*) (texture is not shown here) and in the SmC^* phase. Under a field of 36 V/mm [Fig. 6(b1)], the cell is still uniform, and at 54 V/mm [Fig. 6(b2)], a few domains start to appear from the edges of the cell. At the same applied voltage, the tilt angle in the plot almost reaches a saturation level. The number of domains increased with applied voltage [Fig. 6(b3)] and started to disappear from the side of the edges [Fig. 6(b4)], which is in the unwound state. The domain walls have a single dark line, which means that the lines are accompanied by discrete **c** directors. Here, the point is that the domains appeared for a significantly larger voltage close to the critical voltage for the unwound state. This accords well with the well-known behaviors of the discrete domains in SmC^* [6], where the helix becomes unwound and is accompanied by discrete **c** directors near the critical field. The cell with pure MHPOOCBC in Fig. 5 showed a different behavior. In pure MHPOOCBC, the Sm*A* phase did not show any domains (not shown here), but several domains emerged when the cell was cooled down from the Sm*A* to the SmC^* phase [Fig. 5(a1)]. The domains overlapped but their boundaries did not appear to interfere with each other. This shows that the boundaries of domains are located in different layers. The color is due to the slightly different helical structure for each domain, because the pitch is close to the green wavelength and the optical rotary power is very sensitive to the helical structure when the incident light has a wavelength close to the pitch of the helix. This indicates that the domains are 2π domain walls as pointed out by Pindak *et al.* [16]. The domain boundaries were moved by applying an electric field but the number of them did not change under an applied field of less than 40 V/mm [Fig. 5(a1)]. However, the number of domains increased suddenly near 50 V/mm [Fig. 5(a2)], which corresponds to the field for a sudden rise in the biaxiality, and the domain walls have a single dark line indicating discrete **c** directors. The number of domains continued to increase with the applied voltage [Figs. 5(a3) and 5(a4)], but the domain boundaries became blurred. The domains finally

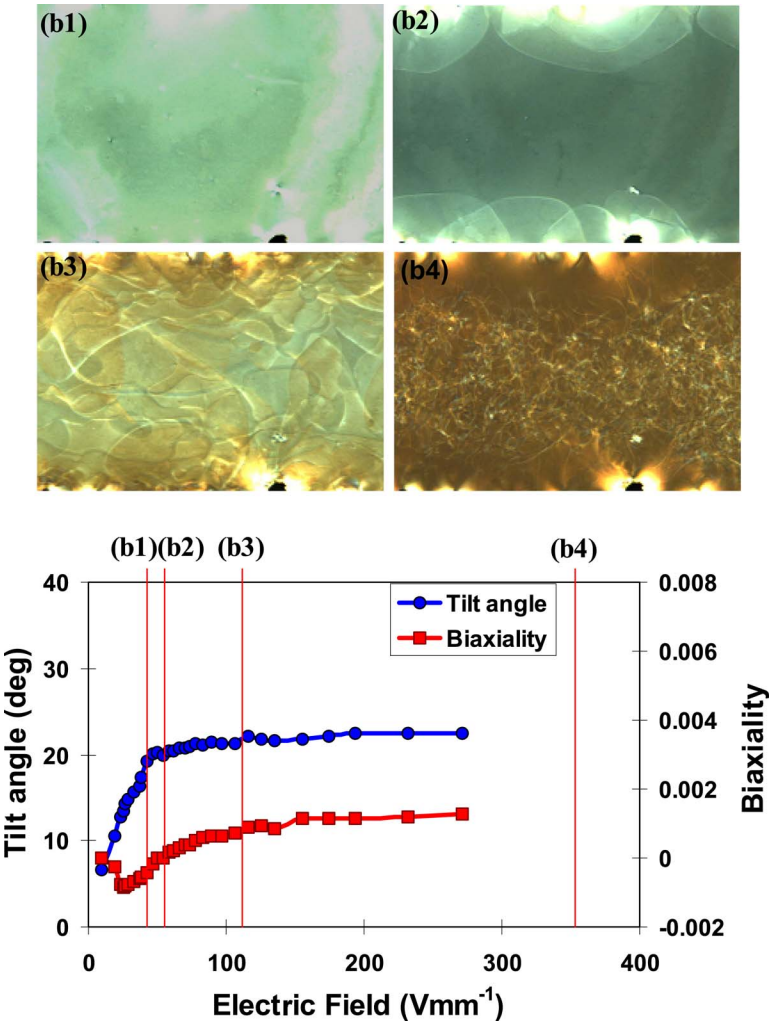

FIG. 6. (Color online) Micrographs (×200) of a homeotropic cell with racemized MHPOOCBC (EE=0.3) at 70 °C: (b1) 36; (b2) 54; (b3) 107; (b4) 375 V/mm.

disappeared at larger voltages, which indicates that the cell has finally reached the unwound state. On decreasing the voltage, the reverse process was observed. To check the reproducibility of the many lines observed in Fig. 5(a2) and to clarify the identification of these lines, another cell with pure MHPOOCBC was prepared. The cell was subjected to a field of 50 V/mm and the same lines as before were observed as seen in Fig. 7(a). Then the field was removed suddenly and the initial state was recovered within a few seconds. We took pictures during the restoration of the initial state as seen in Figs. 7(b)–7(d). [The camera setting condition might be different in the two experiments resulting in slightly different colors in Figs. 5(a1) and 7(d), respectively. So the color purity, that is, the hue, is not the same in the two figures.] The color in Fig. 7(b) indicates that the helix is restored during a very short time, but still many domains do remain. Many domain boundaries, which have a single black line, moved and emerged and disappeared with time. Finally, the cell reached a stabilized state [Fig. 7(d)], which has a few 2π walls. The images show that the cell has many discrete **c** director domains, which means that many lines in Fig. 5(a2) are surely due to the discrete **c** directors.

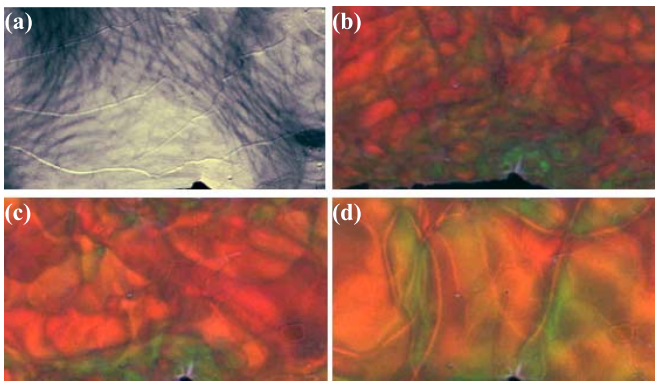

FIG. 7. (Color online) Micrographs (×200) of a homeotropic cell with pure MHPOOCBC at 70 °C; (a) 50 V/mm; (b), (c), and (d) were taken ~0.1 s, ~0.5 s, and ~1.5 s, respectively, after turning off the applied field. Colors are slightly different from those in Fig. 5 due to a different camera setting.

Through the microscopic observations of pure MHPOOCBC, we can see that the discrete **c** director is clearly related to a particular unwinding process of the cell with pure MHPOOCBC, because so many domains were generated at the same field at which a sudden rise in the biaxiality happened. Moreover, the field is much lower than the critical field required for a complete unwinding of the helix. According to the conventional model, discrete **c** directors could appear only near the critical field.

We could observe several domains even at zero field for pure MHPOOCBC in SmC^*, but relatively speaking the smectic layers are coiled uniformly at zero voltage and there are fewer domains. As the field increases, the **c** directors start to move slightly due to the torque $-\mathbf{P}\times\mathbf{E}$ and are populated densely near the direction where the spontaneous polarization **P** is parallel to the electric field **E**, but the number of domains does not increase, that is, the continuity in a single segment is there still. Suddenly, while still at a low voltage, many domains appear, which means that many breaks happen between the adjacent layers, and the continuity in the segment is broken as illustrated in Fig. 14 in the Appendix. The applied field at this stage is much lower than the critical field required for reaching a perfectly unwound state. This looks as if the layers are stuck together so that the molecules in the layers barely twist, but once the persistent coupling between the layers is broken by the electric field, the molecules in the layers can rotate more easily.

This phenomenon can be modeled by adding a narrow energy well in the synclinic position, which is proven to exist in the Appendix. In the conventional model, the continuous **c** director is always expected as seen in Fig. 11 in Sec. IV, because the interlayer interaction energy expressed by the elastic energy increases dramatically on increasing the angle between the two neighboring layers ($\Delta\phi$). This contradicts our experimental results for the presence of the discrete **c** director. As shown in the Appendix, the special behavior of the unwinding process reveals that there exists a narrow energy well in the synclinic position.

III. DISCRETE c DIRECTOR AND A DIFFERENT ELASTIC MODEL

In the helical unwinding process of chiral smectic phases, the angular-dependent free energy of N smectic layers can simply be written in the following form:

$$F=\sum_{i=1}^{N}\left(\frac{1}{2}[U_{i,i-1}(\Delta\phi_{i,i-1})+U_{i+1,i}(\Delta\phi_{i+1,i})]+\frac{\Delta\epsilon' E^2}{8\pi}\cos^2\phi_i - PE\cos\phi_i\right) \tag{5}$$

where $U_{i,i-1}(\Delta\phi_{i,i-1})$ and $U_{i,i+1}(\Delta\phi_{i,i+1})$ denote the interlayer interactions of the ith layer with the $(i-1)$th and $(i+1)$th layers, respectively, as a function of the relative angle $\Delta\phi$ between the two adjacent layers, and the two other terms are the interactions of the dielectric anisotropy ($\Delta\epsilon'=\Delta\epsilon\sin^2\theta$) and the spontaneous polarization (P) of the layers with the applied field, respectively. The in-layer distortion is ignored. By adopting the continuum approximation in the interlayer interaction, $U_{i,i+1}$ can be expressed as the usual elastic distortion energy and Eq. (5) can be written as [5,6]

$$F=\int\left[\frac{K}{2}\left(\frac{d\phi}{dz}-\phi_0'\right)^2+\frac{\Delta\epsilon' E^2}{8\pi}\cos^2\phi-PE\cos\phi\right]dz, \tag{6}$$

where the wave vector $\phi_0'[=2\pi/\text{pitch}]$ is adopted to produce an initial helical structure at zero field, and the discrete summation can be replaced by integration in the continuum approximation. The term for the dielectric coupling is commonly ignored because of its relatively small contribution to the total free energy. Equation (6) has been extensively used for investigating the unwinding process of the SmC^* phase [5,6,9,13,14].

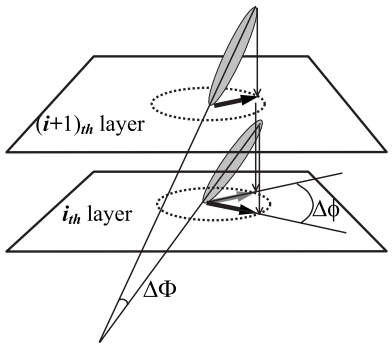

FIG. 8. The angle between the two **c** directors ($\Delta\phi$) and the angle between the two directors ($\Delta\Phi$) in Eq. (7).

When the interlayer interactions in smectic phases are considered, a discrete rather than a continuous model gives a more general solution [3,4]. Moreover, the elastic form of energy in Eq. (6) used **c** directors instead of the molecular directors of liquid crystals and so it is discontinuous at $\Delta\phi_{i,i+1}=\pi$ as seen in Fig. 9, which is surely not realistic. It is quite natural to use the molecular directors for considering the elastic distortion energy. As illustrated in Fig. 8, when the tilt angle is θ and the angle difference between the **c** directors of two neighboring layers is $\Delta\phi$, the actual angle ($\Delta\Phi$) between the two molecular directors (which is not infinitesimally small in the system considered) can be written as

$$\Delta\Phi=2\sin^{-1}\left(\sin\theta\sin\frac{\Delta\phi}{2}\right)\simeq 2\theta\sin\left(\frac{\Delta\phi}{2}\right). \tag{7}$$

This approximation is valid if the tilt angle is not too large. The conventional elastic energy between the ith and $(i+1)$th layers can be written as

$$U_{i,i+1}=\frac{2K}{d^2}\theta^2\sin^2\left(\frac{\Delta\phi_{i,i+1}-\phi_0}{2}\right)=k(\theta)\sin^2\left(\frac{\Delta\phi_{i,i+1}-\phi_0}{2}\right), \tag{8}$$

where $k(\theta)=2K\theta^2/d^2$, K is the usual elastic constant ($\sim 1\times 10^{-6}$ dyne), and d is the thickness of a single layer ($\sim 4\times 10^{-7}$ cm). ϕ_0 is the angle between the adjacent **c** directors at zero field. This equation is continuous near $\Delta\phi=\pi$. It follows the conventional continuum theory except for the discrete notation, and will give the same result in a calculation of the unwinding process.

Now, let us consider the narrow energy well in the synclinic position, which was proven to exist in the previous section. How is such a narrow potential well physically possible? We need to reconsider the first part in Eq. (6), where the elastic energy part of this equation is taken from the nematic continuum theory. Meyer initially suggested Eq. (6) for the unwinding process of cholesteric liquid crystals. This

equation has been used to describe the unwinding process of the SmC^* phase of smectics without any modifications [5,6,9,10] so far. Nevertheless, the interlayer interactions are always present in smectics. The curvature of the director in the nematic phase is continuous and smooth, and so the restoring force is proportional to the curvature strain, which is equivalent to Hooke's law. However, in a smectic structure, the steric energy between the layers is not the same as that in a continuous medium, but should relate to the surface-to-surface interactions. Moreover, many other kinds of interlayer interactions different from the steric ones may also be involved. We can get some ideas from the "sawtooth model" suggested by Glaser and Clark [19] and later verified indirectly by Lee and Lim [20]. In the model, synclinic order is stabilized by the mesh of a set of sawteeth, so the steric energy becomes a minimum in synclinic order, where the sawteeth represent the rough surface of the smectic layers consisting of the tilted terminal parts of molecules. The uneven surface in the model is supposed to be due to the out-of-layer displacements of molecules [21]. Their model suggests that the steric energy at the synclinic position is exceptionally larger than at other positions, which exactly corresponds to our experimental results. Based on the special steric energy concept described as the sawtooth model, we can propose a simple energy model. The depth of the steric energy induced by meshing of the rough surfaces is expected to be proportional to the extent of meshing of the sawteeth with each other. The possibility of the energy having the shape of a Gaussian distribution looks plausible. That is, as the angle departs from the synclinic position, the extent of the surfaces that can mesh with each other is likely to decrease exponentially on either sides of this position. Thus, we can modify Eq. (8) as follows:

$$U_{i,i+1} = k(\theta)\left[\sin^2\left(\frac{\Delta\phi_{i,i+1} - \phi_0}{2}\right) - Ae^{-(\Delta\phi_{i,i+1} - \phi_0)^2/B}\right]. \tag{9}$$

This elastic energy contains an expression for the Gaussian-shaped energy well in the synclinic order in addition to that of the conventional elastic energy, which is plotted in Fig. 9. The dimensionless parameters A and B control the depth and the width of the narrow energy well in the synclinic order.

The elastic constant can be defined as

$$K \equiv \left(\frac{\partial U(\Delta\phi)}{\partial\Delta\phi}\right) \Big/ \Delta\phi. \tag{10}$$

Then the elastic constant of the potential Eq. (9) can be written as

$$K = k(\theta)\left(\frac{\sin\Delta\phi'}{\Delta\phi'} + \frac{2A}{B}e^{-(\Delta\phi')^2/B}\right), \tag{11}$$

where $\Delta\phi' \equiv \Delta\phi_{i,i+1} - \phi_0$. It shows that the elastic constant near synclinic order increases significantly:

$$K = k(\theta)\left(1 + \frac{2A}{B}\right) \quad \text{for } \Delta\phi' = 0,$$

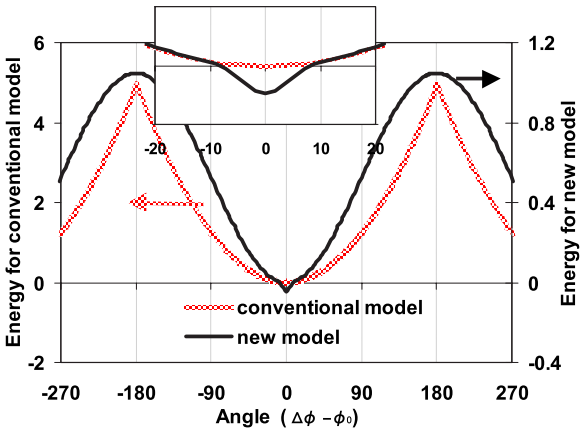

FIG. 9. (Color online) Elastic energy between the adjacent layers using classical elastic energy term [Eq. (6)] and using the new model [Eq. (9), A=0.04, B=0.01, θ=30°], which contains a term for the energy well. The inset shows an expanded view close to the synclinic position. The classical elastic energy and new elastic energy are plotted as $U_{\text{classic}}d^2/K$ and $U_{\text{new}}d^2/K$, respectively.

$$K \simeq k(\theta) \quad \text{for } |\Delta\phi'| \gg 0.$$

The above approximation is valid for $B \ll 1$. This result clearly shows that the surface-surface interactions in synclinic order are much stronger than for any other arrangements.

Equation (5) becomes

$$\frac{F}{k(\theta)} = \sum_{i=1}^{N}\left[\sin^2\left(\frac{\Delta\phi_{i,i+1} - \phi_0}{2}\right) - Ae^{-(\Delta\phi_{i,i+1} - \phi_0)^2/B} - \frac{P}{k(\theta)}E\cos\phi_i\right], \tag{12}$$

where for convenience, both sides have been divided by $k(\theta)$. The dielectric coupling, which is very small, is ignored.

Here, Eq. (12) has the conventional elastic energy as a background to which the Gaussian term for the energy well at the synclinic position has been added. Of course, the conventional form is not complete, because it does not contain the flexoelectric coupling, which is the main cause for the appearance of the various subphases as first suggested by Osipov *et al.* [3], or the dipole-dipole couplings, which were suggested to be a cause of ferro- or antiferroelectric orderings [3,22]. Link *et al.* [17] have also suggested the existence of a minimum energy in the anticlinic order. Many kinds of interlayer interactions may change the sinusoidal background into a more complicated form, which may contain a $\sin^2(\Delta\phi)$ term so that one more minimum appears in the anticlinic order, but we found through a series of simulations that the simple form of Eq. (9) is sufficient to explain the special unwinding behavior, so we will use this simple form for the simulation.

IV. SIMULATION AND DISCUSSION

In this section, we try to confirm the effect of the narrow energy well by using a simple simulation. Equation (12) is

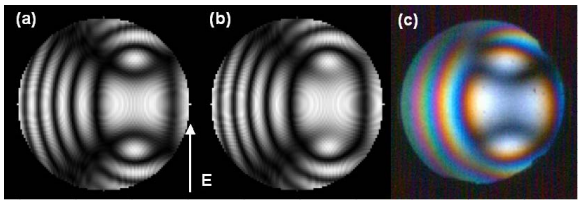

FIG. 10. (Color online) Simulation results (a) and (b) and conoscopic image (c) for MHPOOCBC racemic mixture, EE=0.3, 70 °C, 20 V/mm, verifying validity of the averaged refractive indices method in the long-pitch material having 1.6 μm pitch. (a) Averaged refractive indices method. (b) 4×4 matrix method for 1600 nm pitch; simulation conditions: pitch 1600 nm, cell thickness 40 μm, wavelength 500 nm, layer thickness 4 nm, tilt angle 25°, $n_e=1.7$, $n_o=1.5$, and **c** director distribution shown at $E=10$ V/mm in Fig. 11(a). Here, the cell condition for image (c) is different from the simulation conditions for (a) and (b). The image (c) is to show the typical conoscopic image for the material for EE 0.3 but not for comparison with images (a) and (b).

not easy to solve analytically, so we solve it numerically to obtain the **c** director distributions as a function of the applied field using computer simulations. The initial condition for the simulation is a uniformly coiled state, and on increasing the applied field gradually, the director distributions for the minimum free energy were calculated. For simplification, only one pitch was considered. After acquiring the **c** director distributions, an optical simulation was carried out to obtain the biaxiality and the tilt angle. Thus, the simulation was carried out in two steps; the first step is to calculate the **c** director distributions as a function of the applied field and the second step is to obtain the biaxiality and the tilt angle.

In general, the 4×4 matrix method [13,23] has been used to analyze the optical properties of multilayered structures, but we simplified the calculation process by averaging refractive indices throughout the cell as seen in Eq. (13). In this approximation, the refractive index along the $\hat{\varphi}$ direction in a smectic cell with a complex coiled structure can be obtained by averaging the refractive indices of all layers $[n(\hat{\varphi})_i,\ i=1,2,\ldots]$ along that direction:

$$n^2(\hat{\varphi}) = \langle n^2(\hat{\varphi})_i \rangle_{i=1,2,\ldots}. \tag{13}$$

As already explained in Sec. II, the measured biaxiality and the tilt angle were calculated on the assumption that the pitch is short enough to consider the LC cell as a single biaxial plate. Similarly, the same approximation can be adopted in the simulation by using Eq. (13). We need to verify the validity of the approximation for a mixture with EE value of 0.3, since the pitch of the mixture is ~1530 nm and much longer than the wavelength of light. We simulated the conoscopic images by using a 4×4 matrix and the averaged refractive indices method, and compare the results of those methods in Fig. 10. The simulation conditions are as follows: pitch 1600 nm, cell thickness 40 μm, wavelength 500 nm, layer thickness 4 nm, tilt angle 25°, $n_e=1.7$, $n_o=1.5$, and **c** director distribution at $E=10$ V/mm as given in Fig. 11(a). The two simulation methods give quite similar melatopes, but only the luminance at the optical axes are different. Our

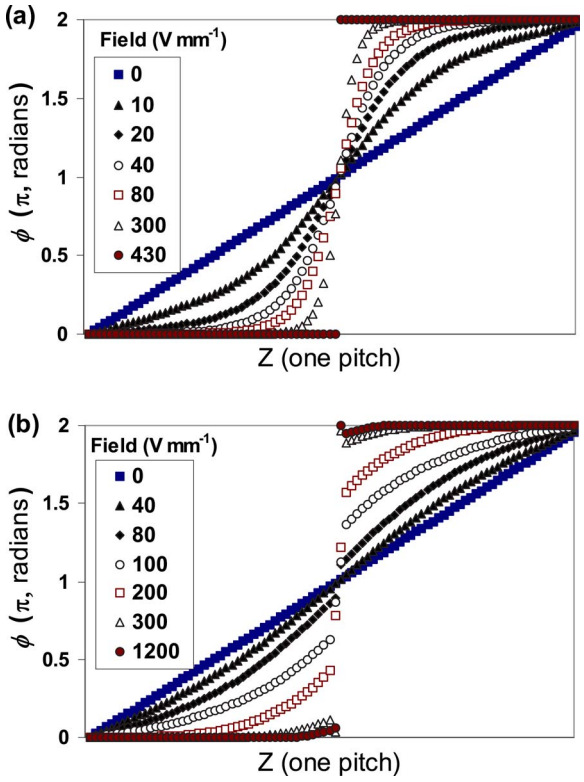

FIG. 11. (Color online) Simulation of directors vs applied field: (a) conventional elastic energy ($A=0$); (b) new model ($A=0.045$). Simulation conditions: 90 layers per pitch, pitch 360 nm, $P/k(\theta)=1.8\times10^{-5}$ nC/dyne, $B=0.01$, tilt angle 25°, $n_e=1.7$, and $n_o=1.5$.

additional simulations (those are not shown in this paper) showed that the averaged refractive indices method is valid up to the pitch of ~2.0 μm, but, as the pitch increases, the image near the optical axes becomes blurred. When the pitch is longer than 3 μm, the conoscopic image becomes quite different and the optical axes are not recognizable. The real conoscopic image [Fig. 10(c)] of the mixture of EE 0.3 has nicely recognizable optical axes, and we can conclude that the single-biaxial-plate assumption for the mixture with EE of 0.3 and the averaged refractive indices method can be used for the analysis of the conoscopic images and the optical simulation.

To verify the effect of a narrow energy well, we carried out simulations by using the above process. The simulation conditions are as follows: the number of layers in a single pitch is 90, pitch is 360 nm, $P/k(\theta)=1.8\times10^{-5}$ nC/dyne, $B=0.01$, tilt angle is 25°, $n_e=1.7$, and $n_o=1.5$. The conditions are selected to be similar to the properties of the pure MHPOOCBC for known parameters such as the number of layers in a pitch, tilt angle, and spontaneous polarization, but for unknown parameters we choose the general values for the smectics. Basically, all other parameters, except for A and B, do not noticeably affect the qualitative unwinding behavior.

The director distributions thus calculated are plotted in Fig. 11, which shows the directions of the **c** directors for each layer in a single pitch. For $A=0$, that is, for the classical elastic energy case, the **c** director orientations are continuous until the unwinding process is completed, while a discrete **c**

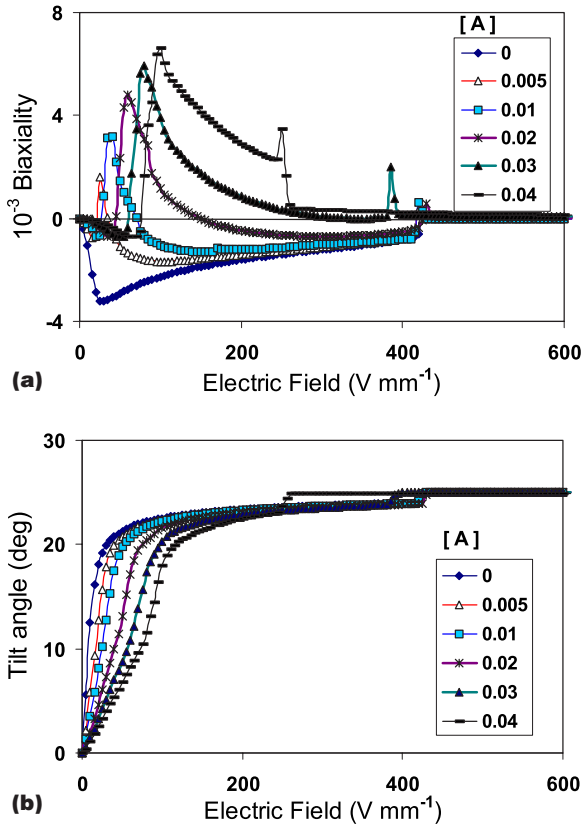

FIG. 12. (Color online) Simulation results for the biaxiality (a) and the tilt angle (b) using new model with the parameter A varied. Simulation conditions: same as those in Fig. 11.

director jump appears at relatively low fields when $A=0.045$. As seen in this simulation, the narrow energy well generates a discrete **c** director distribution during the unwinding of the helix. Figure 12 shows the results of the optical simulation. For $A=0$, it shows negative biaxiality at low voltages and saturates to the unwound state, which is similar to the results at EE 0.3 for a racemized mixture of MHPOOCBC. As the value of A is increased, the field dependence of the biaxiality becomes more like the results for EE 0.7 of MHPOOCBC and finally those of pure MHPOOCBC. The tilt angle results also show a similar behavior. As the value of A increases, a two-step increase in the tilt angle appears, which is similar to the results for the pure MHPOOCBC.

By comparing the two results in Figs. 11 and 12, we arrive at the conclusion that the discrete **c** directors induce a high positive biaxiality. We should recall the microscopic and conoscopic observations of the cells with racemized and pure MHPOOCBC. The cell with racemized MHPOOCBC showed domains near the saturation voltage whereas the cell with pure MHPOOCBC showed the same domains at quite low voltages. Likewise, the cell with racemized MHPOOCBC showed negative biaxiality at low voltages, but the cell with pure MHPOOCBC showed large positive biaxiality. These simulation results indicate that the cell with racemized MHPOOCBC has a shallow energy well whereas the cell with the pure MHPOOCBC has a deep one.

As mentioned in Sec. I, a similar study to find the mechanism for the high positive biaxiality during the unwinding process was carried out by Suwa *et al.* [14]. Based on Eq. (6), Suwa *et al.* found that the biaxiality in the intermediate state of the unwinding of the SmC^* phase became negative by using a simplified molecular distribution model [14]. By using a direct simulation, our results support their conclusion as seen in Figs. 11(a) and 12 (square dot, $A=0$). Thus, the conventional model given by Eqs. (5)–(8) predicts that the biaxiality should be negative during the intermediate state of the unwinding process. Meanwhile, Suwa *et al.* [14] observed large positive biaxiality during the unwinding process of MHPOBC, suggested that a discretely coiled helical structure could be the cause of such a large positive biaxiality, and showed that such a discrete distribution generates a high positive biaxiality through simulation. They could not explain exactly how such a special distribution could appear. They suggested that a discrete distribution of **c** directors might be caused by collaborative contributions from both the ferroelectric and dielectric couplings. The term due to the dielectric contribution is proportional to E^2, while the ferroelectric one is proportional to E. Therefore, as the applied field increases, the dielectric contribution should increase more rapidly than the ferroelectric one. We note that the large positive biaxiality always appears in the range of low fields, whereas it converges to the unwound state due to ferroelectric coupling as the applied field increases. This is confirmed by observing in conoscopy that the tilt plane is perpendicular to the electric field and the tilt angle is equal to one-half of the cone angle. Thus, the unwound state of SmC^* for large applied fields has arisen from the ferroelectric and not from the dielectric coupling. This means that the dielectric coupling compared to its spontaneous polarization counterpart is negligible for small as well as for large fields. Hence, the special unwinding behavior is unlikely to arise from a combination of the dielectric and ferroelectric contributions as was suggested by Suwa *et al.* [14]. Our simulation results clearly show that the large positive biaxiality in the initial stages of the unwinding process is due to the discretely distributed **c** directors, and these discrete **c** director distributions arise from a narrow energy well in the synclinic order.

Now, we try to reproduce the experimental results by using our simulation. However, we may mention that this simulation has some limitations. First, we did not consider the in-layer distortion and the solitary wave propagation in a layer, which may play a role in the unwinding process. Second, we assumed a perfectly uniform helical structure, but the real helical structure consists of many helical segments, each of which has a different length. The averaged spontaneous polarization of each segment is not zero so that each segment rotates even at very low fields. Third, we apply ac square wave voltages at a low frequency of 1 Hz in the real experiment, whereas we assume dc fields in the simulation. Under an ac field, liquid crystal molecules rotate regularly, and the rotation may act as a perturbation and generate more discrete segments. Last, the new model does not represent the energy of the interlayer interactions perfectly as mentioned in the previous section, i.e., it excludes the flexoelectric and the dipole-dipole interactions.

In spite of all those simplifications, the simulated biaxiality and the tilt angle dependencies on field are very similar to

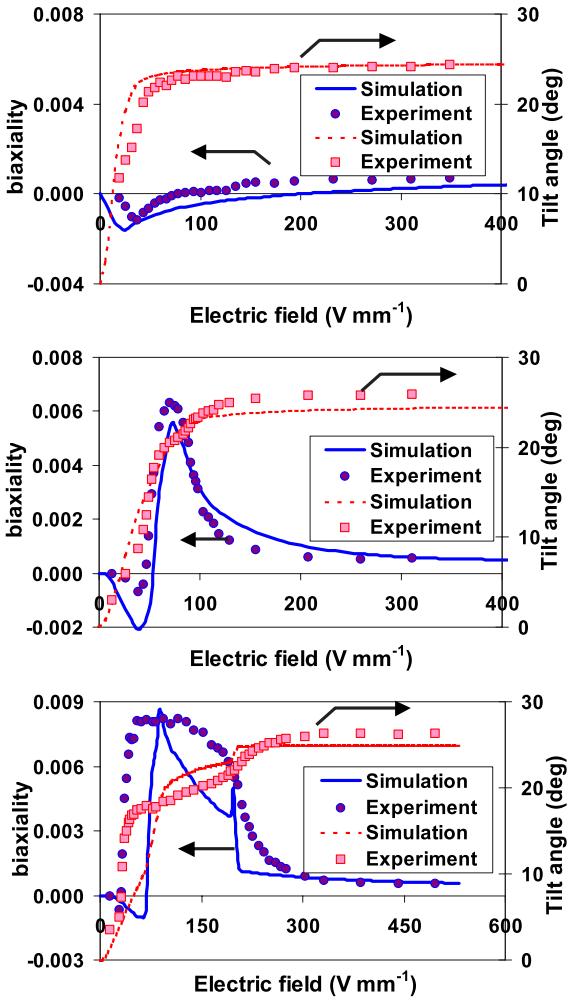

FIG. 13. (Color online) Comparison between the experimental data and the simulation. Experimental data at 60 °C, EE =0.3,0.7,1.0 from the top; simulation conditions: $A=0.001$, 0.03, and 0.045, $P/k=0.4$, 1.4, and 2.4×10^{-5} nC/dyne, and pitch =1440, 720, and 360 nm from the top of the figures, $n_e=1.85$, $n_{o1,o2}=1.5$, 1.501; all other conditions are the same as those in Figs. 11 and 12.

the experimental results as seen in Fig. 13, which shows a comparison between the experimental data and the simulation results. Simulation conditions in the top graph are ($A=0.001$, $B=0.01$, $P/k=0.4\times10^{-5}$ nC/dyne, 360 layers per pitch, pitch 1440 nm), middle ($A=0.03$, $B=0.01$, $P/k=1.4\times10^{-5}$ nC/dyne, 180 layers per pitch, pitch 720 nm), and bottom ($A=0.045$, $B=0.01$, $P/k=2.4\times10^{-5}$ nC/dyne, 90 layers per pitch, pitch 360 nm), and the refractive indices are $n_e=1.85$, $n_{o1,o2}=1.5$, 1.501, respectively.

These clearly show that the various unwinding behaviors are due to the existence of a narrow energy well in the synclinic order, and the depth of the energy well depends on the enantiomeric excess ratio and the temperature. The higher the racemization ratio (that is, the more pure the liquid crystal), the deeper the energy well. This can easily be explained intuitively, through a semiempirical term. The energy well is located at $\Delta\phi-\phi_0=0$, that is, $\Delta\phi=\phi_0$, which generates helical structure. Intuitively, this helical structure is due to the chirality and this results in the terminal parts of molecules being slightly tilted away from the tilt plane. Opposite-handed molecules may have oppositely tilted terminal parts, and they disturb the meshing of two sawteeth. Therefore, by mixing opposite-handed molecules, we can decrease the depth of the narrow energy well. The temperature dependence can also be explained in a similar way. As the temperature increases, thermal fluctuations become stronger, and these consequently are reflected in a reduction of the depth of the energy well.

From the simulation result, we can obtain another important conclusion. For pure MHPOOCBC, the elastic constant expressed by Eq. (11) is around ten times higher at $\Delta\phi'=0$ than that at other angles. The sawtooth effect intensifies the interlayer steric energy in synclinic ordering and increases the elastic constant.

V. CONCLUSION

The helical unwinding process has been studied in the SmC^* phase of MHPOOCBC. Results for the biaxiality and for the tilt angle have been obtained as a function of the electric field for various enantiomeric excess ratios varying from 0.3 to 1.0. A tilted conoscopic method has been developed, where the biaxiality in the SmC^* phase can be measured up to a tilt angle of 45°. The conventional continuum theory, where the restoring force is proportional to the curvature of the directors, adapted from cholesteric liquid crystals subjected to an electric field to the helical unwinding of smectic phases by many researchers [5,6,9] has been examined. We find that the continuum theory cannot adequately explain the helical unwinding of smectic phases. This conclusion is natural because the coupling between the layers in smectics is quite different from the director curvatures in the continuum theory. Conoscopic and microscopic observations of pure and racemized MHPOOCBC reveal the existence of a narrow energy well in the synclinic order. Due to this energy well, the helical structure is likely to be broken more easily into segments rather than unwound continuously by an external field. Computer simulation using this energy model showed that the depth of the energy well affects the biaxiality sensitively during the unwinding process. By drawing a comparison between the simulation and the experimental results, we conclude that the depth of the energy well decreases on mixing with oppositely handed molecules. This indicates that the steric energy between the adjacent surfaces formed by the slightly tilted terminal parts of molecules is the origin of the energy well, and the surfaces are disturbed by the opposite-handed molecules. Because of this effect, the elastic constant near synclinic order is expected to be roughly ten times higher than for any other arrangement of the molecules in adjacent layers.

ACKNOWLEDGMENTS

We thank the Science Foundation of Ireland (SFI) Grant No. 02/IN.1/I.031 for funding the research work in Dublin. Professor A. Fukuda and Dr. A. D. L. Chandani are thanked

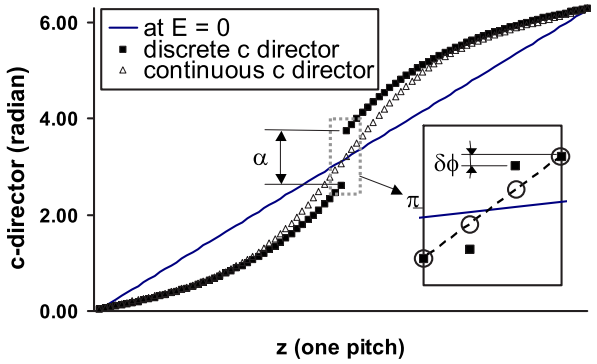

FIG. 14. (Color online) Plots of the discrete and the continuous **c** directors. A small part in the middle is enlarged. In the inset, solid square is for discrete **c** directors and open circle is for continuous **c** directors when considering only four layers.

for valuable discussions. J.K.S. thanks Samsung Electronics Co., Ltd. for granting the leave of absence from Seoul.

APPENDIX: PROOF OF THE EXISTENCE OF AN ENERGY WELL IN THE SYNCLINIC POSITION

In this appendix, we prove that there exists a narrow energy well in the synclinic position on the assumption that the helical structure is broken into segments at quite low fields as explained in the text.

Figure 14 illustrates the distribution of the continuous and discrete **c** directors along the helical pitch. Let us consider only four layers around the discrete point. In the continuous **c** director condition (open circles in the inset of Fig. 14), the **c** directors of the four layers are separated at the same angles. Meanwhile, in the discrete **c** director condition (solid squares in the inset of Fig. 14), the angle (α) between the second and third layers is far greater than that between the first and second and the third and fourth layers ($\delta\phi \sim \phi_0$).

From the basic assumption, we can conclude that

$$\sum_{i=1}^{4} f_{i,C} > \sum_{i=1}^{4} f_{i,D}. \tag{A1}$$

Here, $f_{i,C}$ and $f_{i,D}$ are the free energies of the ith layer under the continuous and discrete **c** directors, respectively. We can use Eq. (5) to solve Eq. (A1):

$$\begin{aligned} &-PE\left[2\cos\left(\pi+\frac{\alpha}{2}+\delta\phi\right)+2\cos\left(\pi+\frac{\alpha}{6}+\frac{2\delta\phi}{6}\right)\right] \\ &\quad+3U\left(\Delta\phi=\frac{\alpha}{3}+\frac{2\delta\phi}{3}\right) \\ &>-PE\left[2\cos\left(\pi+\frac{\alpha}{2}+\delta\phi\right)+2\cos\left(\pi+\frac{\alpha}{2}\right)\right] \\ &\quad+2U(\Delta\phi=\delta\phi)+U(\Delta\phi=\alpha). \end{aligned} \tag{A2}$$

For simplification, the coupling of the dielectric anisotropy with the applied field was ignored. By expanding the cosine terms and ignoring higher-order terms, Eq. (A2) can be written as

$$U\left(\Delta\phi=\frac{\alpha}{3}+\frac{2\delta\phi}{3}\right) > \frac{2U(\Delta\phi=\delta\phi)+U(\Delta\phi=\alpha)}{3} - \frac{2}{27}\alpha^2 PE. \tag{A3}$$

Here, the last term is quite small compared with the other terms. Let us compare the $U(\Delta\phi=\alpha)/3$ and $(2/27)\alpha^2 PE$ terms:

$$\frac{(2/27)\alpha^2 PE}{U(\Delta\phi=\alpha)/3} \simeq 1.0\times 10^{-4} \ll 1. \tag{A4}$$

In this calculation, we use

$$U(\Delta\phi)=\frac{K}{2}\left(\frac{\Delta\phi}{d}\right)^2,$$

$$E_c=\frac{\pi^4 K}{4L^2 P},$$

$$L \simeq 100d,$$

$$E \simeq \frac{E_c}{10}.$$

The critical voltage E_c is derived by Meyer [5], and the pitch L is roughly 100 times the thickness of a single layer, d, in this material.

Since the last term is negligibly small, Eq. (A3) can be written as

$$U\left(\Delta\phi=\frac{\alpha+2\delta\phi}{3}\right) > \frac{2U(\Delta\phi=\delta\phi)+U(\Delta\phi=\alpha)}{3}. \tag{A5}$$

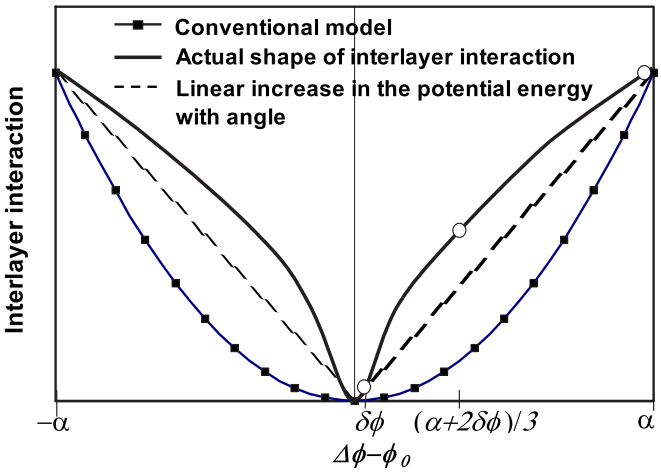

FIG. 15. (Color online) Shape of the potential energy curve close to the synclinic position. Note that the shape of the potential curve at the synclinic position has significantly altered compared to the conventional curve.

Equation (A5) shows that the potential energy at a point one-third of the way between $\Delta\phi = \delta\phi$ and α (here, $\alpha \gg \delta\phi$) is higher than a linearly increasing line between $\Delta\phi = \delta\phi$ and α. This means that the potential energy curve has a decreasing inclination between the two points, as shown in Fig. 15.

Considering that α is much smaller than π at the initial stage of the generation of the discrete **c** directors, the energy well is located at the synclinic position and the width is quite narrow.

Thus, we can conclude that the generation of the discrete **c** director proves the existence of a narrow energy well in the synclinic position for interlayer interactions.

[1] A. Fukuda, Y. Takanishi, T. Isozaki, K. Ishikawa, and H. Takezoe, J. Mater. Chem. **4**, 997 (1994).

[2] A. D. L. Chandani, N. M. Shtykov, V. P. Panov, A. V. Emelyanenko, A. Fukuda, and J. K. Vij, Phys. Rev. E **72**, 041705 (2005).

[3] M. A. Osipov, A. Fukuda, and H. Hakoi, in Proceedings of the Anglo-Japanese Joint Workshop, Southampton, 2000 [Mol. Cryst. Liq. Cryst. **402**, 9 (2003)].

[4] N. M. Shtykov, A. D. L. Chandani, A. V. Emelyanenko, A. Fukuda, and J. K. Vij, Phys. Rev. E **71**, 021711 (2005).

[5] R. B. Meyer, Mol. Cryst. Liq. Cryst. **40**, 33 (1977).

[6] P. G. de Gennes and J. Prost, *The Physics of Liquid Crystals*, 2nd ed. (Clarendon Press, Oxford, 1993), Chap. 7.

[7] J. K. Song, A. D. L. Chandani, O. E. Panarina, A. Fukuda, J. K. Vij, V. Goertz, and J. W. Goodby, Ferroelectrics **344**, 41 (2006).

[8] J. K. Song, A. D. L. Chandani, A. Fukuda, J. K. Vij, I. Kobayashi, and A. V. Emelyanenko (unpublished).

[9] L. A. Parry-Jones and S. J. Elston, Phys. Rev. E **63**, 050701(R) (2001).

[10] N. Baytch, R. L. B. Selinger, J. V. Selinger, and R. Shashidhar, Phys. Rev. E **68**, 041702 (2003).

[11] E. Gorecka, A. D. L. Chandani, Y. Ouchi, H. Takezoe, and A. Fukuda, Jpn. J. Appl. Phys., Part 1 **29**, 131 (1990).

[12] T. Matsumoto, A. Fukuda, M. Johno, Y. Motoyama, T. Yui, S. S. Seomun, and M. Yamashita, J. Mater. Chem. **9**, 2051 (1999).

[13] S. Suwa, H. Hoshi, Y. Takanishi, K. Ishikawa, H. Takezoe, and B. Zeks, Jpn. J. Appl. Phys., Part 1 **42**, 1335 (2003).

[14] S. Suwa, Y. Takanishi, H. Hoshi, K. Ishikawa, and H. Takezoe, Liq. Cryst. **30**, 499 (2003).

[15] P. E. Cladis, H. R. Brand, and P. L. Finn, Phys. Rev. A **28**, 512 (1983).

[16] R. Pindak, C. Y. Young, R. B. Meyer, and N. A. Clark, Phys. Rev. Lett. **45**, 1193 (1980).

[17] D. R. Link, G. Natale, J. E. Maclennan, N. A. Clark, M. Walsh, S. S. Keast, and M. E. Neubert, Phys. Rev. Lett. **83**, 3665 (1999).

[18] P. V. Dolganov, B. M. Bolotin, and A. Fukuda, Phys. Rev. E **70**, 041708 (2004).

[19] M. A. Glaser and N. A. Clark, Phys. Rev. E **66**, 021711 (2002).

[20] J. H. Lee and T. K. Lim, J. Appl. Phys. **98**, 094110 (2005).

[21] Y. Takanishi, A. Ikeda, H. Takezoe, and A. Fukuda, Phys. Rev. E **51**, 400 (1995).

[22] A. A. Murauski, Ferroelectrics **344**, 117 (2006).

[23] D. W. Berreman, J. Opt. Soc. Am. **62**, 502 (1972).